Phase diagram of the two-dimensional complex Ginzburg–Landau equation

Hugues Chaté [a,b], Paul Manneville [b,a]

[a] *CEA – Service de Physique de l'Etat Condensé, Centre d'Etudes de Saclay, 91191 Gif-sur-Yvette, France*
[b] *LadHyX – Laboratoire d'Hydrodynamique, Ecole Polytechnique, 91128 Palaiseau, France*

Abstract

After a brief introduction to the complex Ginzburg–Landau equation, some of its important features in two space dimensions are reviewed. A comprehensive study of the various phases observed numerically in large systems over the whole parameter space is then presented. The nature of the transitions between these phases is investigated and some theoretical problems linked to the phase diagram are discussed.

The complex Ginzburg–Landau equation (CGL) is one of the most important simple nonlinear partial differential equations for two main reasons. First, as we will briefly recall below, it arises as the natural description of many physical situations, or at least is the "kernel" of many systems of amplitude equations. Second, its solutions display a very rich spectrum of dynamical behavior when its parameters are varied, reflecting the interplay of dissipation, dispersion and nonlinearity.

Here, we give a brief and mostly qualitative report of the various regimes observed in the two-dimensional case, and discuss several theoretical aspects of these numerical findings.

1. Introduction to CGL

A large body of work has already been devoted to the CGL equation, which reads

$$\partial_t A = A + (1 + ib_1)\nabla^2 A - (b_3 - i)|A|^2 A, \tag{1}$$

where A is a complex field.

In the context of amplitude equations [1,5], which are large-scale descriptions of physical systems past (and near) symmetry-breaking instability thresholds, the CGL
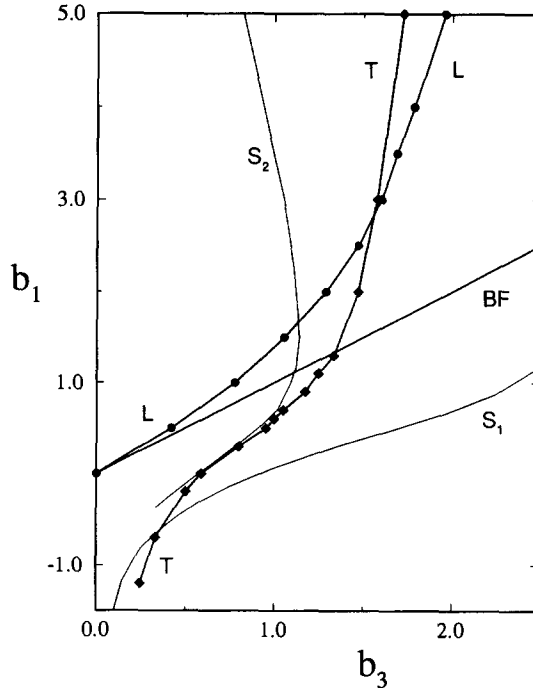
Fig. 1. Phase diagram of the two-dimensional CGL equation. Phase turbulence is observed between lines L and BF, defect turbulence to the left of line T, and frozen states exist (approximately) to the right of line S_2. Details are given in the text.

equation has been recognized as the relevant equation for the slow modulations of oscillations in a continuous medium near a Hopf bifurcation [2]. More generally, it appears in the description of spatially-extended systems when oscillations or waves are present.

Under the form (1), the CGL equation has been reduced (without loss of generality) to its simplest from, with only two real parameters, b_1 and b_3. The first term of the rhs is related to the linear instability mechanism which led to oscillations. The second term accounts for diffusion and dispersion, while the cubic nonlinear term insures – if $b_3 > 0$, otherwise other terms may be necessary – the saturation of the linear instability and is involved in the renormalisation of the oscillation frequency. Two important limits are worth mentioning: when $b_1 = 0, b_3 \rightarrow \infty$, one has the real Ginzburg–Landau equation, which possesses a Lyapunov functional and thus exhibits only relaxational dynamics [3]. When $b_1 \rightarrow \infty, b_3 = 0$ dispersion plays the essential role, as one recovers the nonlinear Schrödinger equation [4]. In the general case, sustained spatio–temporally disordered regimes are observed in large regions of the parameter plane (Fig. 1).

The genericity of the CGL equation, associated to its relative simplicity, has made it one of the favorite playgrounds for testing ideas about spatio–temporal chaos in a rather realistic context [5]. It is only recently, though, that a comprehensive study has been undertaken, as it was realized that away from the intricacy of the bifurcation diagrams at

small sizes, there exists a crossover size beyond which chaos becomes extensive and can be characterized by intensive quantities independent of system size, boundary conditions, and, to a large extent, initial conditions [6]. Indeed, when chaos is extensive, statistical approaches are legitimate and should provide rather simple descriptions. In this context, bifurcation diagrams – typically used for small dynamical systems – are replaced by "phase diagrams" delimiting the regions of different statistical signatures in parameter space.

Whereas the one-dimensional case is now rather well known [7–9], the situation in two dimensions is much less satisfactory, mainly because previous work was devoted to punctual problems rather than to acquiring a global picture of the properties of the equation. Here, thanks to current computer power, we provide a comprehensive overview of the two-dimensional CGL equation in the large-size limit[1].

2. Waves, phase instability and defects

We now introduce a few important features of the CGL equation before proceeding to the description of the phase diagram.

Early work on CGL has dealt with the problem of the linear stability of its family of plane-wave solutions $A = a_k \exp i(kx + \omega_k t)$ with $a_k^2 = (1 - k^2)/b_3$ and $\omega_k = 1/b_3 - (b_1 + 1/b_3)k^2$. All these solutions are unstable for $b_1 > b_3$ (Newell criterion), a condition which defines the so-called "Benjamin–Feir" (BF) line (Fig. 1). For $b_1 < b_3$, plane-wave solutions with $k^2 < k_{max}^2 = (b_3 - b_1)/(3b_3 - b_1 + 2/b_3)$ are linearly stable [10]. The instability of the travelling wave solutions above the BF line is readily verified as to be linked to the "gauge" invariance of the equation, i.e. its invariance by an arbitrary phase shift ($A \rightarrow A \exp i\phi_0$). Near the BF line, the amplitude modes are strongly damped, "slaved" to the marginal phase mode, so that one often speaks of a *phase instability*. This instability has been conjectured to lead to a disordered regime called *phase turbulence* [11], in which the field A never reaches zero, so that the phase $\phi = \arg A$ is defined everywhere. Near the BF line, the phase gradient $\nabla \phi$ is expected to remain small, and a systematic expansion can be performed, leading to a description of the large-scale dynamics in terms of the phase only. The behavior of the resulting series of *phase equations* obtained by truncation of this expansion is actually not very well known, except for the Kuramoto–Sivashinsky (KS) equation to which these equations reduce infinitely close to the BF line. If phase turbulence (i.e. spatio–temporal chaos) has been established for the KS equation, it is the subject of an ongoing controversy away from the BF line, both for the phase equations and for the CGL equation itself [11,9,12,13].

---

[1] A previous study (see [21]), using a discretized version of the CGL equation, attempted such a task. In view of the results presented here, it appears that the effects of the discretization scheme on the phase diagram are rather drastic. In particular, no phase turbulence regime was observed by these authors, an artifact, we believe, due to their numerical scheme. Other discrepancies will be discussed elsewhere [18].

Another important feature of the CGL equation is the structure, nature, and role of "defects", i.e. points in space–time where $A = 0$. At such points, the phase is not defined, and it varies by a multiple of 2π when going around them. For space dimensions $d \geq 2$, defects are topologically constrained. This has been recognized for a long time as one of the salient features of the two-dimensional CGL [14,15]. For $d = 2$, defects are points and can only appear and disappear by pairs. For small enough b_1 values, they appear in two different types, "spirals" and "shock-line vertices" (Fig. 2). The shock-line vertices have mostly been considered as "passive" objects which play no important role. However accurate this statement may be, it remains that the spiral defects have attracted the most attention [15,16]. In spite of all these efforts, no exact expression is available; on the other hand, much is known about the core structure and the "wings", i.e. the emitted outward-going waves. Away from the core, these waves are asymptotic to a planewave with a well-defined wavenumber k_{sp} depending only on b_1 and b_3. The stability properties of the $k = k_{sp}$ planewave solution give rise to two important lines in the (b_1, b_3) parameter plane. On the S_1 line, $k_{sp} = k_{max}$, the maximum wavenumber of linearly stable planewaves (Fig. 1). This line delimits the region of linear stability of the $k = k_{sp}$ wave. To its left, the wave is linearly unstable (perturbations grow exponentially in phase space); this is in fact a *convective* instability: a *localized* perturbation indeed grows, but is advected away from its initial position at the group velocity of the $k = k_{sp}$ planewave. At this initial position, the solution relaxes to the planewave. According to Aranson et al. [16], the $k = k_{sp}$ planewave becomes *absolutely* unstable to the left of the S_2 line: any initial perturbation grows at its initial location (in addition to spreading in the direction of the wave).

It is not exactly known how these stability limits of the planewave with wavenumber k_{sp} are related to the actual stability properties of the spiral solution and to its observability in an experimental context. In most of the region of the parameter plane considered here, the spiral solution exists and is core-stable [17]. In consequence, it can be argued that its stability properties are essentially related to those of the asymptotic $k = k_{sp}$ planewave in a *semi-infinite* domain (with the core sitting at one end). We now formulate, at a somewhat conjectural level, the stability properties of the spiral solution and their consequences observable in experiments (be they numerical or not). To the right of line S_1, one expects the spiral to resist a (small) amount of noise, due to its "complete" (core and wings) linear stability. Between S_1 and S_2, perturbations are amplified but convected away from the core at the group velocity of the $k = k_{sp}$ solution. Numerical experiments have shown that the spiral is most sensitive to perturbations in the crossover region between the core and the wings [18]. At a given level of (experimental) noise, perturbations coming from this region are the most dangerous ones. This convective instability in fact takes the form of growing oscillations of the *modulus* $|A|$ as one goes away from the core (see Fig. 6). Experimentally, these oscillations do not saturate, and the wave breaks down, creating more defects. This mechanism defines a maximum radius R_{noise} which limits the size of observable spirals, and depends on the instability rate and (weakly) on the noise level. Approaching the limit of absolute instability (line S_2), this diameter goes to zero, and beyond S_2 the spiral is "completely"
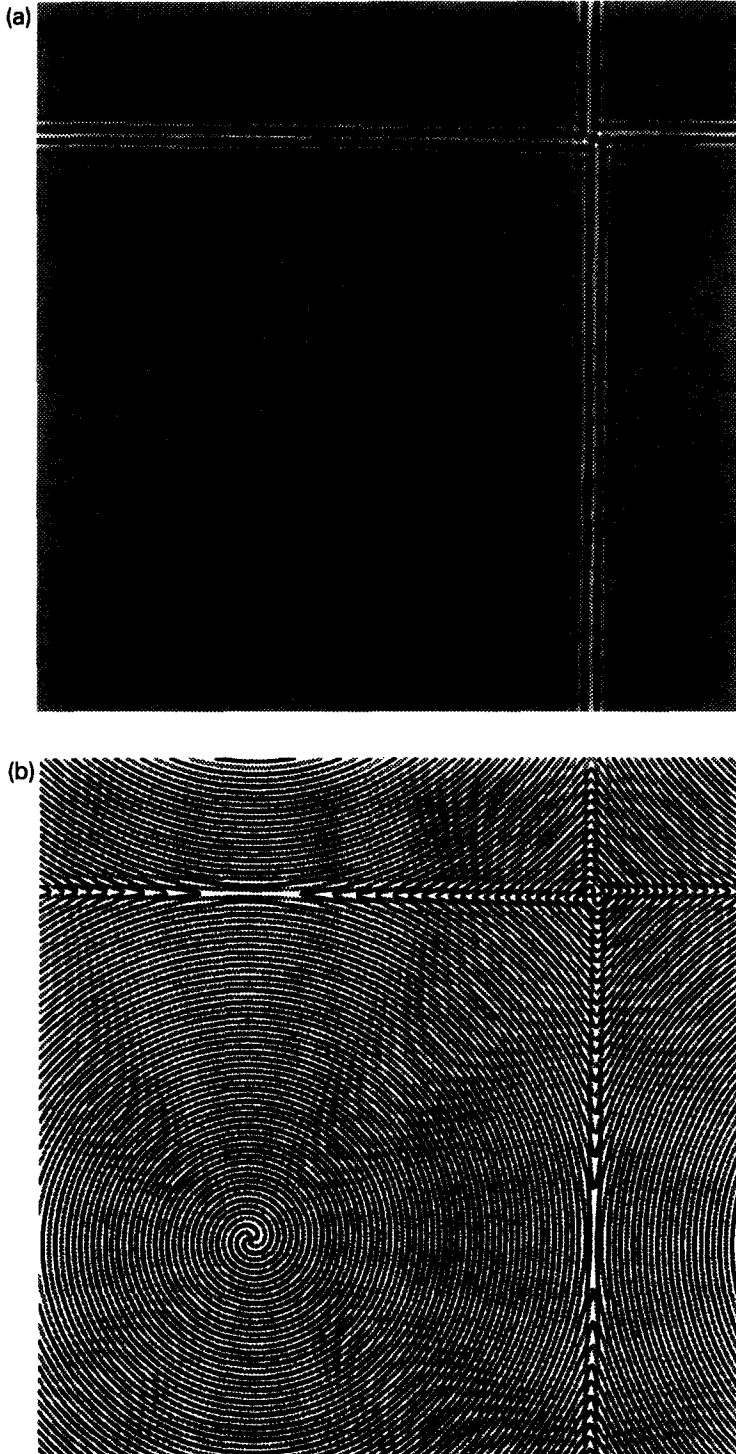
Fig. 2.

unstable and cannot be observed in an experimental (noisy) context.

Finally, we note that if defects do play an important role in the two-dimensional CGL equation, as we will show below, their topological character is not crucial in determining the dynamical regimes: for $d = 1$, localized "quasi-defects" – where $|A|$ remains locally very close to zero – have been shown to be the key-ingredient in some disordered regimes [8]. But the topological constraint on defects for $d \geq 2$ does provide them with a large domain of existence in parameter space, insuring their relevance in most of the regimes of interest.

3. Phases

Fig. 1 shows the phase diagram of the two-dimensional CGL equation established from a numerical exploration of systems of linear size of the order of $L = 512$ with periodic boundary conditions, using a pseudospectral code. Details about the integration scheme and the numerical protocol will be given elsewhere [18]. The various transition lines are discussed in detail in Section 4.

As in the one-dimensional case [7,8], two types of disordered regimes can be distinguished, depending on whether they exhibit defects or not. To the right of the line L in the parameter plane, *phase turbulence* (no defects) is observed, whereas *defect turbulence* occurs to the left of line T.

3.1. Phase turbulence

Between the BF and the L lines, spatio–temporally chaotic regimes of phase turbulence – where no defect occurs – are observed. With periodic boundary conditions, the total phase gradient across the system (the "winding number") is conserved. This introduces a new invariant to the problem. Most results reported here (in particular the location of line L) are for the case of zero winding number.

In phase turbulence, the solution consists of a disordered cellular structure, (best seen in plots of $|A|$ or $\nabla\phi$) slowly evolving in time (Fig. 3a). The typical size of the cells diverges like $(b_3 - b_1)^{-1/2}$ when approaching the BF line; this size is in fact of the order of the wavelength of the most unstable mode in the corresponding KS equation. If the correlations of the modulus $|A|$ still decay rapidly, those of the phase ϕ decay slowly, with power-law-like behavior. This is apparent in the large-scale modulations of the phase field (Fig. 3b). In Section 5, we discuss the effective large-scale model for phase turbulence and the asymptotic behavior of the correlations in phase turbulence.

Fig. 2. Snapshot of a simple frozen configuration with one spiral defect and one shock-line defect. System of size $L = 512$ with periodic boundary conditions and parameters $b_1 = 2$ and $b_3 = 1.67$. (a): image of $|A|$ in grey scale from $|A| = 0$ (black) to $|A| = 1.33$ (white); (b): lines $\text{Re}(A) = 0$ (light grey) and $\text{Im}(A) = 0$ (dark grey).

(a)

(b)

Fig. 3.

Even though they are certainly important to better understanding the dynamics of phase turbulence, the "elementary processes" at play in this regime are not known. For $d = 1$, it has been shown that propagative structures are the objects triggering the breakdown of phase turbulence [9]. Here, no equivalent has so far been found (see below). One should also investigate whether the evolution of the cellular structure involves some of the elementary events observed in the coarsening of soap froths [19] (even though these cannot account for all the dynamics here, since the cellular structure is statistically stationary). Knowledge of the local dynamics is necessary to build a large-scale effective description of two-dimensional phase turbulence in the spirit of the work of Chow and Hwa [20] for the one-dimensional KS equation.

3.2. Defect turbulence

Defect turbulence is the most chaotic regime of the two-dimensional CGL equation: correlations decay exponentially, with short correlation lengths and times. Depending mostly on b_1, the space–time signature of the solutions varies. For large b_1, the density of defects is large, they come and go rapidly, and they rarely form spirals (Fig. 4).

Indeed, it can be argued that defects *per se* are not crucial features in this case. "Amplitude turbulence" is a better name for such spatio–temporal chaos regimes. Furthermore, increasing b_1 toward the nonlinear Schrödinger equation limit, *pulses* become the relevant objects: the solutions consist of localized regions where $A \neq 0$. Approaching the BF line, the defect density decreases, the characteristic scales increase, and spirals can be observed. In fact well-developed spirals can only be observed in the defect turbulence region, to the right of the S_2 line (see the discussion of the transition lines in the next section).

3.3. Frozen states

Cellular structures also appear in the two-dimensional CGL equation in the form of quasi-frozen arrangements of spiral defects surrounded by shock lines. In these states, the field $|A|$ is generally completely stationary in time. The network of these lines form the cells of these spatially-disordered states (Fig. 5). Non-spiral defects lie at the shock-line vertices, sometimes also along the shock lines themselves, in metastable arrangements. Because the timescales involved are very long, it is actually difficult to decide when these structures stop evolving. Residual, intermittent, local rearrangements – less and less frequent along time – are observed, and this relaxation process is reminiscent of that taking place in glasses. In fact, much remains to be done in order to decide to what

Fig. 3. Snapshot of phase turbulence in a system of linear size $L = 5120$ with periodic boundary conditions and parameters $b_1 = 2$ and $b_3 = 1.33$. (a): field $|A|$ in a sub-system of linear size $\ell = 640$; grey scale from $|A| = 0.87$ (black) to $|A| = 1.12$ (white); (b): phase field $\phi = \arg A$ in the whole system (grey scale from black to white over the total range of variation of the phase $\Delta\phi \sim 4.27$) .
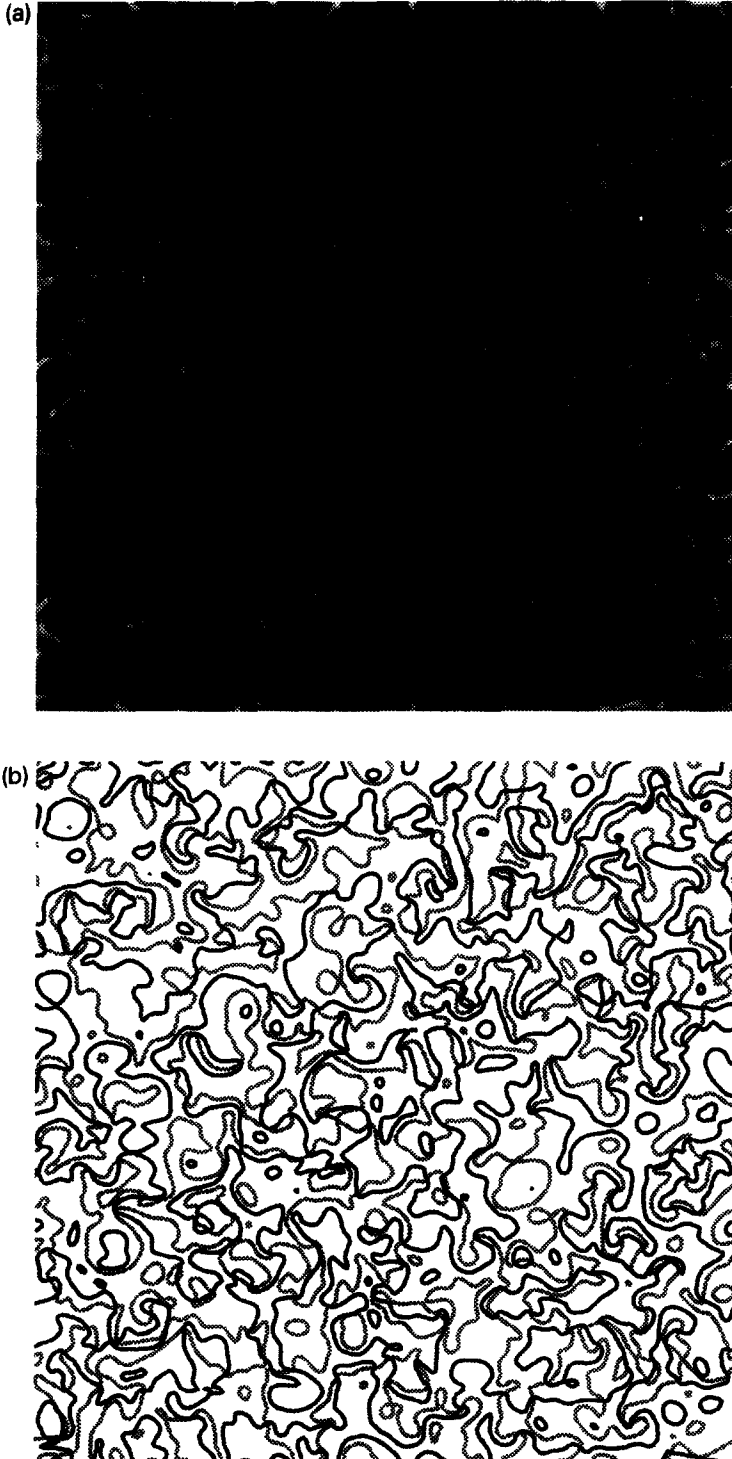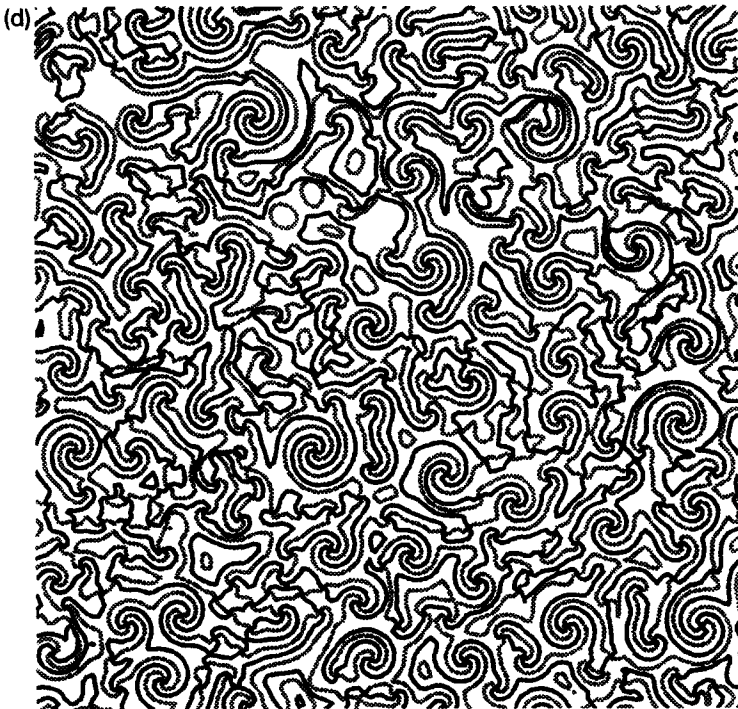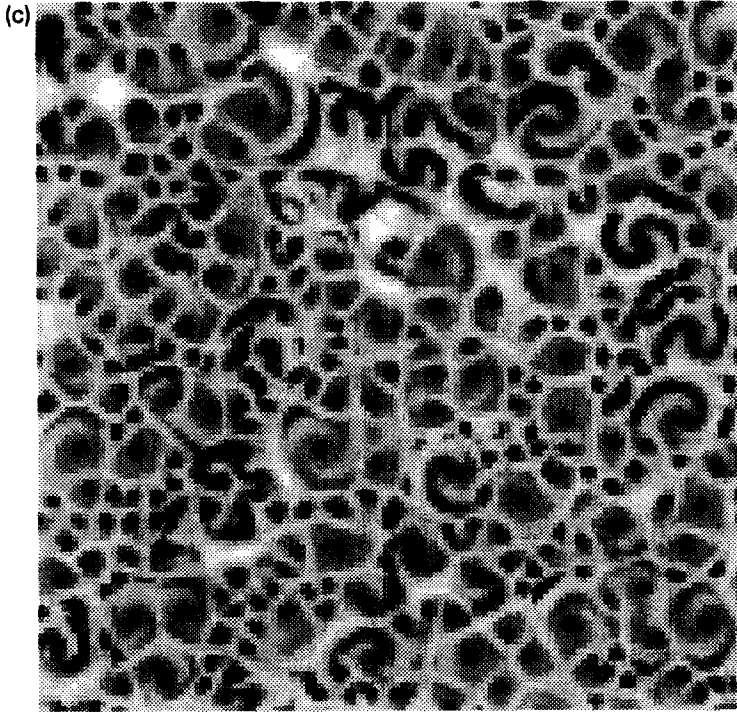
Fig. 4. For caption see p. 359.
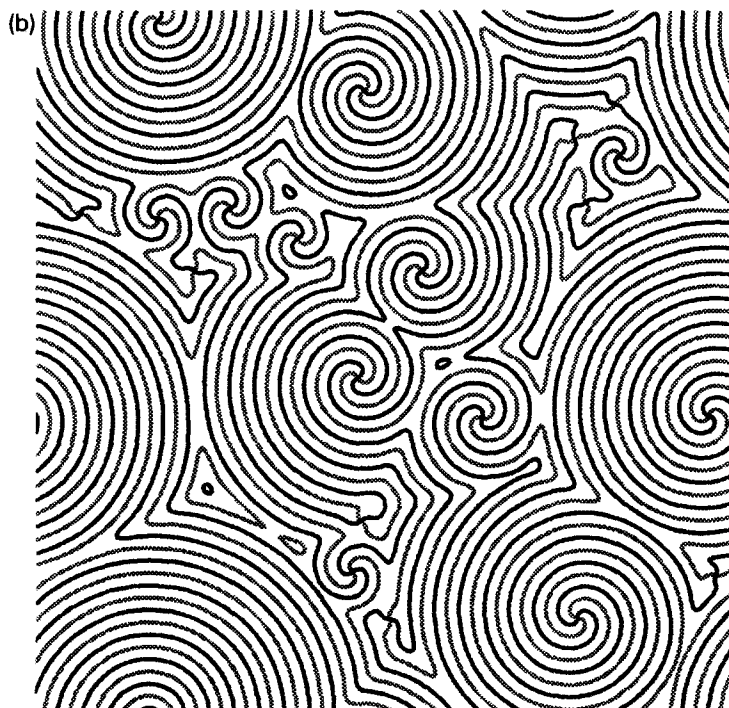
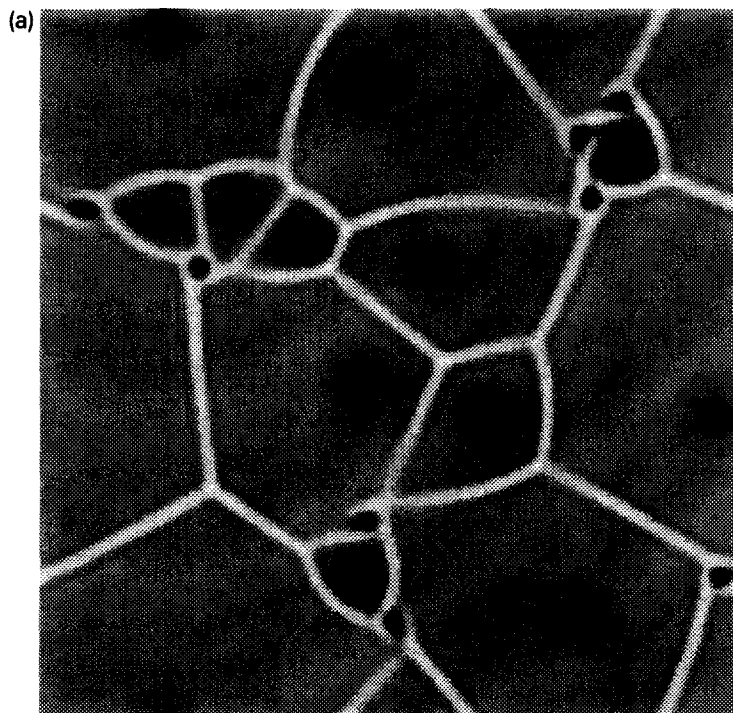Fig. 4 — continued.

(a)

(b)

Fig. 5.

extent these dynamical states are glassy states. A first study along these lines can be found in Huber [21]. A particular point of interest is to investigate whether some kind of aging phenomena are taking place in these frozen structures.

The frozen states are easily observed in the region of the parameter space to the right of line T, where they are the only asymptotic solutions possessing defects. Their total domain of existence in the (b_1, b_3) plane can be estimated on the basis of the stability properties of spirals, as discussed in Section 2. The frozen states do not exist to the left of line S_2, since there the spirals are absolutely unstable. On the other hand, nothing precludes their existence to the right of S_2. The size of the cells is not limited, except in the presence of noise, since in this case, between S_2 and S_1, spirals have a maximum radius R_{noise}. In practice, the dynamical "history" which led to a given frozen structure greatly influences the distribution of sizes of cells in the structure (see the discussion in Section 4.1 below).

The actual observation of frozen states in the region between lines S_2 and T, where defect turbulence exists, is not easy, though, because these states are metastable with respect to defect turbulence. Coming, for example, from a frozen asymptotic state to the right of line T, the parameters have to be changed "adiabatically" to prevent the nucleation of defect turbulence. Even then, the necessary rearrangements of the cellular structure, which involve the rapid motion of some defects, most often trigger the "melting" of the frozen structure. Frozen structures are most easily observed far to the right of line T, and especially to the right of S_1. Their domain of existence probably extends to large values of b_3 (except maybe for large $|b_1|$). At any rate, along the $b_1 = 0$ axis, it extends to the real Ginzburg–Landau ($b_3 \to \infty$) limit, where the spirals become the vortex excitations of the XY model [22].

4. Transitions

The respective domains of existence of the three disordered phases described above are delimited by the lines BF, T, L, and S_2. We discuss now the nature of the various (phase) transitions observed when crossing these lines and comment on the relative stability of the disordered phases.

Fig. 4. Snapshots of defect turbulence in a system of linear size $L = 256$ with parameters $(b_1, b_3) = (2, 1)$ (a),(b) and $(b_1, b_3) = (0, 0.56)$ (c),(d). There are 268 defects in the first case, but no well-formed spirals are observed; in the second case, on the other hand, spirals are clearly visible. (a): field $|A|$; grey scale from $|A| = 0$ (black) to $|A| = 1.32$ (white); (b): Re(A) = 0 (light grey) and Im(A) = 0 (dark grey) lines; (c): field $|A|$; grey scale from $|A| = 0$ (black) to $|A| = 1.0$ (white); (d): Re(A) = 0 (light grey) and Im(A) = 0 (dark grey) lines.

Fig. 5. Frozen state in a system of linear size $L = 256$ with parameters $b_1 = 2$ and $b_3 = 5$. (a): field $|A|$; grey scale from $|A| = 0$ (black) to $|A| = 1.17$ (white); (b): lines Re(A) = 0 (light grey) and Re(A) = 0 (dark grey).

H. Chaté, P. Manneville/Physica A 224 (1996) 348–368
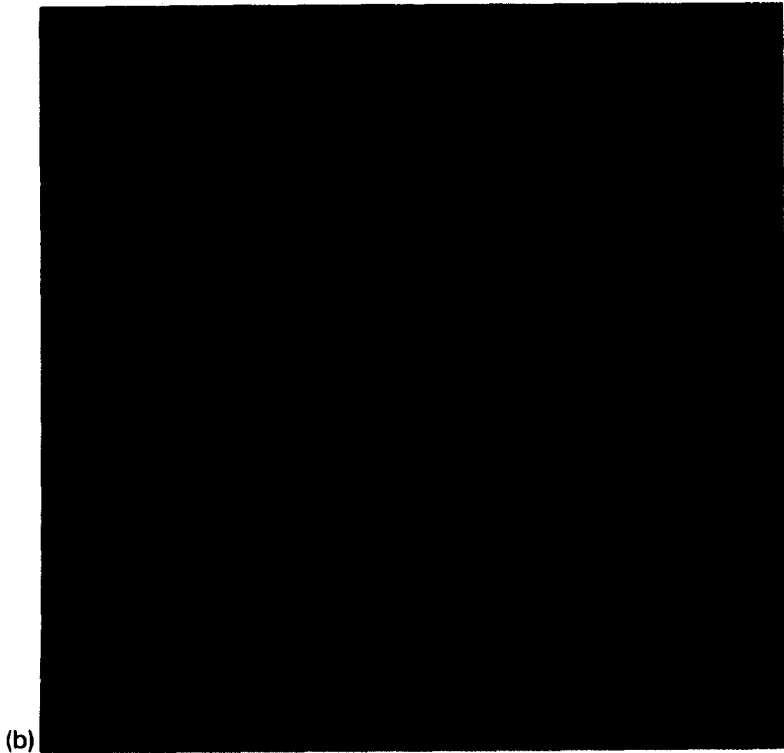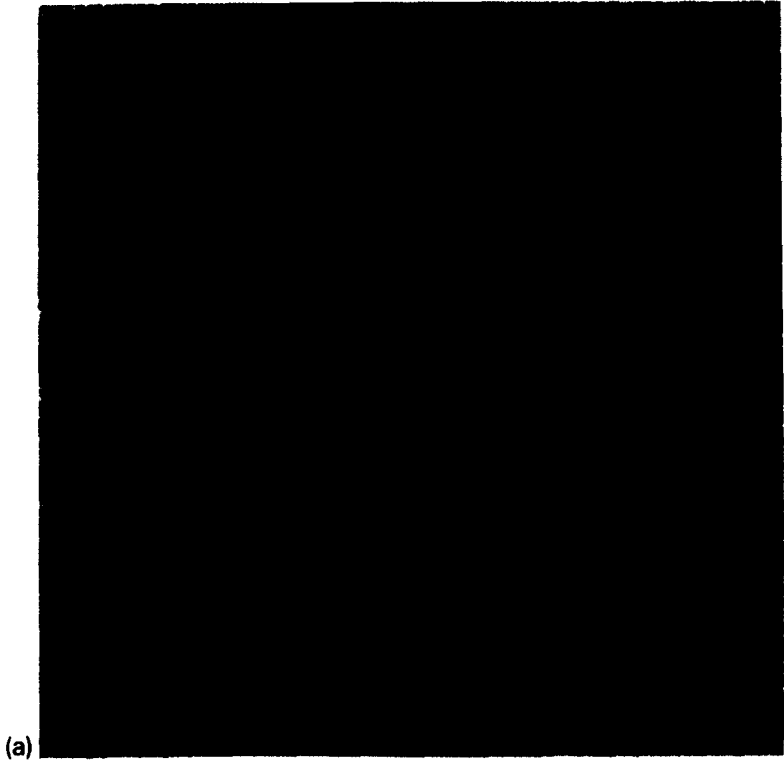

(a)

(b)

Fig. 6.

4.1. Lines T and S₂

As already mentioned, line T delimits the (numerically estimated) domain of existence of *sustained* regimes of defect turbulence. Starting from a defect turbulence regime, *increasing* b_3, this highly chaotic regime is maintained until line T is crossed; defect turbulence is only transient then, and is followed by the nucleation of a frozen state (Fig. 6). As observed by Huber et al. [21], this transition is indeed reminiscent of a first-order phase transition. Depending both on the amplitude of the "quench" beyond line T (i.e. the distance of the current parameters to line T) and the b_1 value of the crossing point, the duration of the transient varies widely. The smaller the quench and the larger b_1, the longer the transient. As a matter of fact, line T can be seen as the line where this transient is infinite.

The nucleation process involves the appearance of a sufficiently large spiral core. To the right of line T, the spiral may then grow, but its size is limited to a maximum radius R_{turb} (Fig. 6a). This radius results from the interaction between the outward-going spiral waves and the strong, finite-amplitude fluctuations characteristic of the defect turbulence "bath" surrounding it. These fluctuations trigger the most unstable mode of the spiral solutions, i.e. the oscillations of $|A|$ which are the signature of the nonlinear stage of the convective instability, and influence the spiral wave *inward*. We stress that this is different from the problem usually considered when studying convective instabilities. Here a semi-infinite convectively-unstable medium is put in contact "downstream" with a turbulent medium. The balance between the (destabilizing) turbulent fluctuations and the (regularizing) advection of perturbations by the spiral waves takes place at the nonlinear level, so that the radius R_{turb} cannot be determined from the stability properties of the spiral alone [18].

Approaching line T from the right, R_{turb} decreases. Numerical experiments [18] show that the line T′, where $R_{turb} = 0$ (not shown in Fig. 1), is located to the *left* of line T. Note that, in contrast with line T, line T′ is defined *via* a local dynamical phenomenon. In the region between lines T and T′, "fully developed" defect turbulence decays to mixed states, i.e. mostly-frozen structures in which some localized patches of turbulence subsist (Fig. 6b). Numerically speaking, this residual turbulence does not seem to vanish at long times; extensive statistical data has to be compiled in order to decide whether this remains true in the infinite-time limit, in which case lines T and T′ are distinct. In the other case, one must conclude that line T, in the thermodynamic limit, moves to

Fig. 6. Nucleation of a frozen state from defect turbulence in a system of linear size $L = 1024$ with parameters $b_1 = 2$ and $b_3 = 1.33$. (a): two spirals have been nucleated and have reached their maximal size $R_{turb} \sim 225$; (b): asymptotic state consisting of a frozen structure of spirals with maximum radius R_{turb} with some residual turbulence for $L = 1024$, $b_1 = 2$, and $b_3 = 1.43$. This asymptotic state is typical of the region between lines T and T′ (compare with Fig. 5). (Snapshots of field $|A|$, color scale from $|A| = 0$ (dark red) to $|A| = 1.22$ (light yellow)). Note the oscillations of $|A|$ away from the spiral cores, near their maximum radius, which are the signature of the convective instability of the $k = k_{sp}$ planewave.

the left to coalesce with line T'. However, in a similar fashion to what happens with line L in phase turbulence (see next section), line T is numerically well-defined for all practical purposes, and it is only a theoretical point to know whether it is distinct from T' in the infinite-time limit. We note finally that the frozen states nucleated this way (i.e. from the spontaneous decay of defect turbulence) possess a maximal cell size given by R_{turb}.

The transition from defect turbulence to frozen states is hysteretic: coming from a frozen state, and *decreasing* b_3, it is, in principle, possible to keep *completely* frozen structures past line T, (even if "partially" frozen structures, such as the one shown in Fig. 6b, coexist in the region between lines T and T'). As mentioned in Section 3, line S_2 is only an absolute and approximate limit of the hysteresis region: in theory, the effects of the curvature of the waves and the spiral core should be taken into account, and in practice, in this region of parameter space, the frozen states are easily destroyed by perturbations, so that it is extremely difficult to observe the frozen states far to the left of line T. In fact, the real limit of existence of frozen states might be actually determined by the properties of the *nonlinear* stage of the convective instability of the waves and possibly also by the stability properties of the shock-line vertices, the other key-component of frozen structures. This very intricate situation will be examined in detail in [18]. The distance between lines T and S_2 is thus only an approximate measure of the *maximal* width of the hysteresis loop.

4.2. Line L

Line L is the (numerically-determined) line beyond which (to its left) phase turbulence is only transient. To its right, phase turbulence can be observed for as big a system and as long a time as current computers allow. A brief discussion of the existence of phase turbulence in the infinite-size, infinite-time limit is given in the next section, but, numerically speaking, line L is rather well defined, with the probability of breakdown of phase turbulence being finite to its left and essentially zero to its right.

The breakdown of phase turbulence is also a nucleation process (Fig. 7).

A pair of defects is nucleated by some fluctuation on one side of a cell, triggering a "chain-reaction" leading to the quasi-deterministic invasion of the system by a growing bubble of the defect turbulence phase. The diameter of this bubble increases linearly with time (Fig. 7d).

A priori, three sections of line L have to be considered, delimited by the crossing points with lines T and S_2 (or, rather, the line actually delimiting the existence of frozen states). Below line T, the only possible regime is defect turbulence, so that the breakdown of phase turbulence can only lead to this regime. Between lines S_2 and T, defect turbulence and frozen states coexist, and the breakdown could lead to either state. In fact, the nucleation events at the origin of the breakdown are always highly chaotic, and only defect turbulence arises (this is not surprising, considering the metastability of frozen states in this region). The third portion of line L, above its crossing with line T, offers an interesting possibility: there, only frozen states are expected asymptotically. But

the breakdown of phase turbulence first triggers a defect turbulence transient which then itself nucleates a frozen state. No direct transition from phase turbulence to frozen states seems possible, although it is conceivable that one might observe, in a large system, a nucleating frozen state within the growing bubble of defect turbulence invading phase turbulence.

Finally, we note, not surprisingly, that the breakdown of phase turbulence is also an hysteretic transition. Crossing line L from left to right, one remains in either defect turbulence or a frozen state.

5. Discussion

After this brief description of the "phase diagram", we comment on important related points as well as some theoretical problems currently under investigation.

5.1. Infinite-size, infinite-time limit

The phase diagram of Fig. 1 summarizes numerical results. As such, even though customary precautions have been taken (e.g. to insure the extensivity of chaos in the disordered regimes), it does not represent the "true" phase diagram, i.e. that of the infinite-size, infinite-time, "thermodynamic" limit. This question, which also arises in the $d = 1$ case, has been recently investigated [13], in particular with respect to the existence of phase turbulence in the thermodynamic limit (represented by line L here). Indeed, the very existence of phase turbulence is questioned. As for the $d = 1$ case, it is currently impossible to make a definitive statement, on the basis of numerical simulations alone, as to whether line L coalesces with the BF line in the thermodynamic limit. A careful analysis of statistical data about phase turbulence in one and two dimensions for various system sizes and integration times is under way and will be reported elsewhere [18]. Extrapolation of size effects, though, seems to lead to the conclusion that phase turbulence might not exist in the thermodynamic limit. It remains nevertheless that for all practical purposes (numerical or experimental), there exists a domain of parameter space where phase turbulence is statistically stationary and subsists – even in very large systems – for times as long as desired. At any rate, Fig. 1 is representative of system sizes and integration times accessible to current computers (say up to linear size L in the order of 10^4 and integration times up to 10^5), and line L is probably slightly shifted for much larger systems.

The status of line T, which delimits the domain of existence of sustained regimes of defect turbulence, is subjected to similar remarks. Statistical data about the probability of breakdown (to a frozen state) should be cumulated in order to estimate the position of line T in the thermodynamic limit. This should be completed by a detailed study of the variation of R_{turb} with parameters b_1 and b_3 to provide a precise determination of line T'. The question, raised in Section 4.1, of whether lines T and T' coalesce in the thermodynamic limit, could thus be addressed. The existence of defect turbulence is not in question, though, as line T is bound to be situated to the right of line S_2 (which limits absolutely the domain of existence of frozen states).
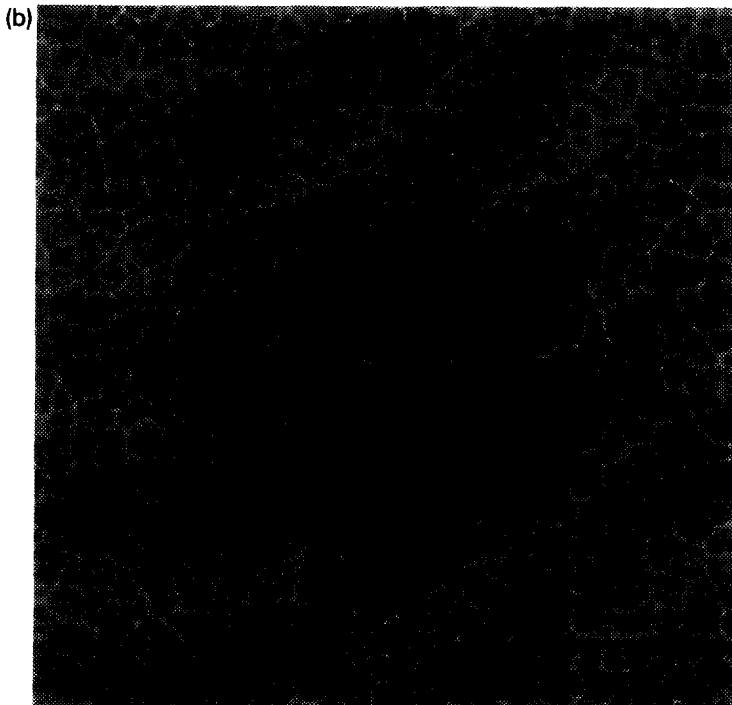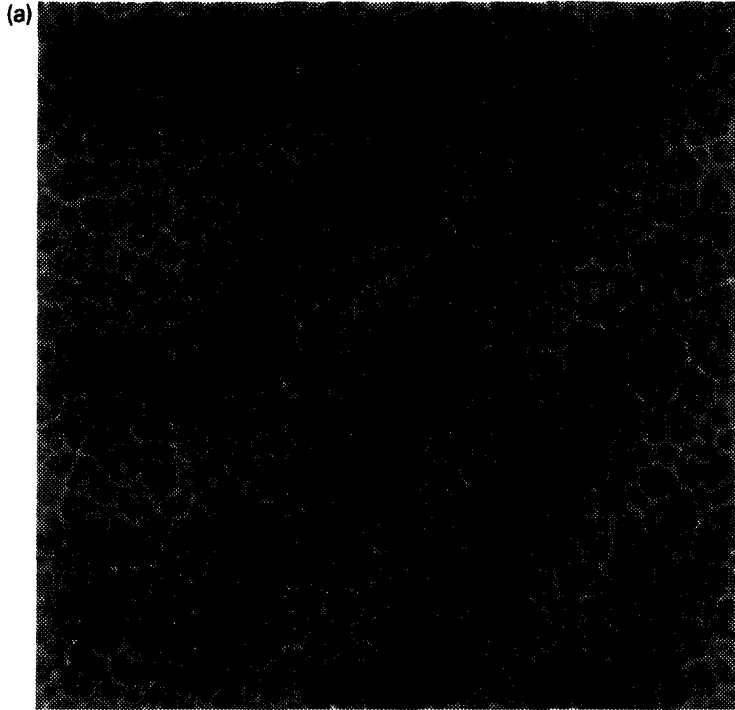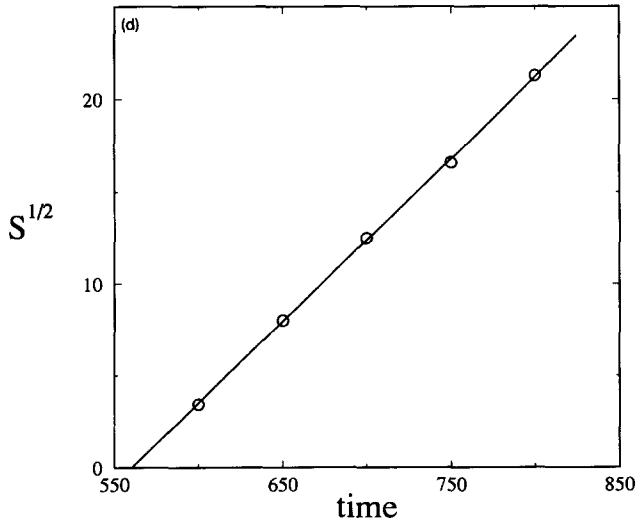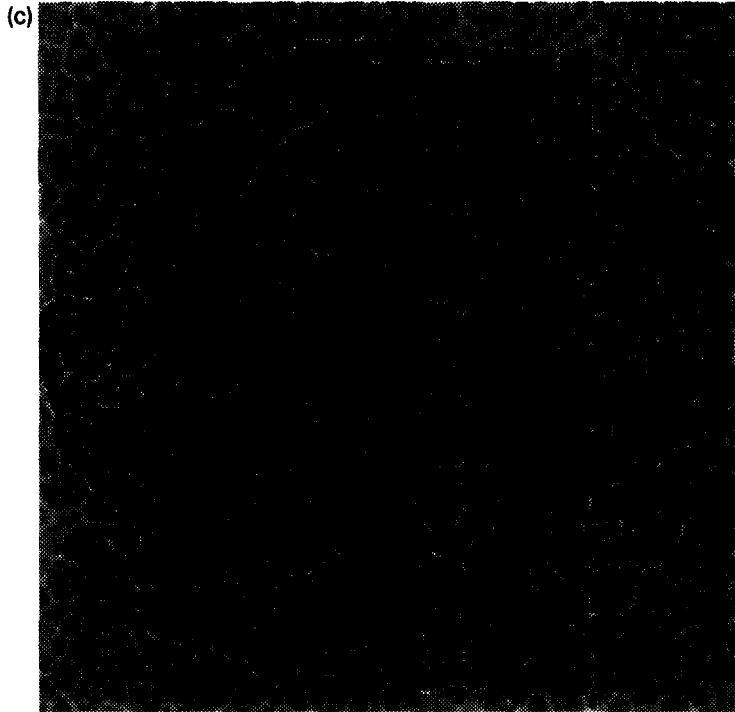
Fig. 7. (a),(b)

Fig. 7. Breakdown of phase turbulence in a system of linear size $L = 512$ with parameters $b_1 = 2$ and $b_3 = 1.28$ coming from a phase turbulent system at $b_1 = 2$ and $b_3 = 1.33$. (a)–(c): snapshots of field $|A|$ at time $t = 600, 700, 800$ in grey scale from $|A| = 0$ (black) to $|A| = 1.29$ (white). Note the growing "bubble" of defect turbulence, whose diameter increases linearly with time ((d): square root of the surface S of the bubble along time).

5.2. Cellular structures

Cellular structures appear both in phase turbulence (Fig. 3) and, of course, as frozen states (Fig. 5). In phase turbulence, the dynamics produces statistically stationary configurations which can be studied along the lines of what is usually done for, say, the coarsening of soap froths [19]. For example, a first step would be to estimate the statistical properties of cells – their sizes, their number of sides – and a second stage could consist in determining the local events of which their dynamical evolution is composed. As mentioned in Section 3.2, this should provide a better understanding of the elementary processes involved in phase turbulence, as well as a better statistical description of this regime. This could also pave the way to a simple "particle model" sharing the same statistical properties, similar to the work of Rost and Krug [23] on the KS equation. In the case of the frozen states, as discussed earlier, the characteristics of the structures depend strongly on the "dynamical history" that led to them, so that an investigation of their geometrical properties must be correlated to their origin and formation.

5.3. Complete phase diagram

Admittedly, the phase diagram of Fig. 1 is not quite complete. Work remains to be done, in particular on the following points:
- The $b_1 \to \infty$, "nonlinear Schrödinger", limit needs to be clarified: Where are lines S_2 and T located? How does the *core* instability of spirals intervene in the dynamical regimes?
- The $b_1 < 0$ region, and especially the prolongation of line T, should be investigated, as well as the $b_1 \to -\infty$ limit.
- It is known that, at least for $d = 1$, the CGL equation exhibits well-behaved disordered regimes in some parts of the $b_3 < 0$ half-plane [24], in spite of the absence of the usual nonlinear saturation mechanism. Such a possibility should also be explored in the two-dimensional case.
- The processes of nucleation of the spiral cores should be studied in detail, at least from a statistical point of view. In particular, the minimal core size that can possibly lead to the growth of a spiral should be estimated, as well as the probability of such an event. This would help define a line to the right of line T beyond which nucleation is immediate (corresponding to the line "NUC" in [21]), as well as clarify the nature of the frozen states with residual turbulence observed experimentally between lines T and T'.

5.4. Large-scale description

The possibility of large-scale descriptions of deterministic spatio–temporal chaos in terms of Langevin-like, (nonlinear) stochastic equations, is a question currently being debated, essentially because one can then hope to apply methods of statistical mechanics [25]. One central point is to investigate to what extent and under what conditions the local chaotic fluctuations are equivalent to a "noise" at large scales.

The CGL equation offers, here also, a good testground for such questions. In this spirit, phase turbulence has been proposed [26] to be described, at large scales, by the noisy Burgers or Kardar–Parisi–Zhang (KPZ) [27] equation, which is (among other things) a model for the kinetic roughening of stochastic interfaces. Indeed, since the phase $\phi = \arg A$ is always defined in this regime, one can consider the evolution of the phase field only (at least on an experimental level), which, in turn, can be seen as the progression of a d-dimensional interface in a $(d + 1)$-dimensional medium (unwinding the phase advance on the real axis). Numerical results for $d = 1$ and $d = 2$ seem to confirm the validity of the KPZ ansatz [18]. The KPZ picture also reveals the asymptotic behavior of correlations in phase turbulence. In particular, spatial correlations of the phase should decrease either algebraically ("linear regime" of KPZ) or like a stretched exponential ("nonlinear regime").

To go beyond this type of numerical observation, the effective large-scale stochastic equation has to be built from the original model. An important step toward this aim has been achieved recently for the one-dimensional Kuramoto–Sivashinsky equation (which is also believed to be described by KPZ at large scales [28]). Carefully studying the elementary mechanisms at the origin of spatio–temporal chaos, Chow and Hwa [20] have succeeded in calculating, from data on local chaos only, the parameters of the effective KPZ equation. It is not clear how such a program could be carried out for the CGL equation in any of its disordered regimes – even for phase turbulence – but a detailed analysis of the elementary processes at work in each case appears as a necessary step deserving further work.

6. Conclusion

The general picture of the two-dimensional CGL equation presented here, even though it should be completed along the lines mentioned above, already provides a good starting point to people wanting to study various aspects of spatio–temporal chaos in this system. In particular, our study should help choose specific parameter values. It should also help experimentalists recognize whether the physical or numerical problems they study are typical of the CGL equation and, if so, of what particular regime. Finally, natural extensions of this work include a similar study of the three-dimensional case, and of the various modifications of CGL usually considered in the literature.

References

[1] See, e.g., A.C. Newell, Envelope equations, in: Nonlinear Wave Motion, Lectures in Applied Mathematics, Vol. 15 (American Mathematical Society, Providence, RI, 1974) p. 157.
[2] Y. Kuramoto, Chemical Oscillations, Waves and Turbulence (Springer, Tokyo, 1984);
J. Lega, Défauts topologiques associés à la brisure de l'invariance de translation dans le temps, Thèse de doctorat, Université de Nice (1989);
W. van Saarloos, The complex Ginzburg–Landau equation for beginners, in: Spatiotemporal Patterns in Nonequilibrium Systems, P.E. Cladis and P. Palffy-Muhoray, eds. (Addison-Wesley, Reading, MA, 1994).
[3] See, e.g., R. Graham, Phys. Rev. A 10 (1974) 1762.

[4] See, e.g., A.C. Newell, Rocky Mountains J. Math. 8 (1978) 25;
    A.C. Scott, F.Y.F. Chu and D.W. McLaughlin, Proc. IEEE (1973) 1443;
    Y.S. Kivshar and B.A. Malomed, Rev. Mod. Phys. 61 (1989) 762;
    A.C. Newell, D.A. Rand and D. Russell, Phys. Lett. A 132 (1988) 112;
    S. Popp, O. Stiller, I. Aranson and L. Kramer, Physica D 84 (1995) 424.

[5] M.C. Cross and P.C. Hohenberg, Pattern formation outside of equilibrium, Rev. Mod. Phys. 65 (1993) 851.

[6] D.A. Egolf and H.S. Greenside, Nature 369 (1994) 129.

[7] B.I. Shraiman, A. Pumir, W. van Saarloos, P.C. Hohenberg, H. Chaté and M. Holen, Physica D 57 (1992) 241;
    A. Pumir, B.I. Shraiman, W. van Saarloos, P.C. Hohenberg, H. Chaté and M. Holen, Phase vs. defect turbulence in the one-dimensional complex Ginzburg–Landau equation, in: Ordered and Turbulent Patterns in Taylor–Couette Flows, C.D. Andereck, ed. (Plenum Press, New York, 1992).

[8] H. Chaté, Nonlinearity 7 (1994) 185.

[9] H. Chaté, Disordered regimes of the one-dimensional complex Ginzburg–Landau equation, in: Spatiotemporal Patterns in Nonequilibrium Systems, P.E. Cladis and P. Palffy-Muhoray, eds. (Addison-Wesley, Reading, MA, 1994).

[10] B. Janiaud, A. Pumir, D. Bensimon, V. Croquette, H. Richter and L. Kramer, Physica D 55 (1992) 259.

[11] H. Chaté and P. Manneville, Phase turbulence, in: Turbulence: A Tentative Dictionary, P. Tabeling and O. Cardoso, eds. (Plenum, New York, 1994), and references therein.

[12] H. Sakaguchi, Prog. Theor. Phys. 84 (1990) 792.

[13] D.A. Egolf and H.S. Greenside, Phys. Rev. Lett. 74 (1995) 1751.

[14] P. Coullet, L. Gil and J. Lega, Phys. Rev. Lett. 62 (1989) 1619;
    L. Gil, J. Lega and J.L. Meunier, Phys. Rev. A 41 (1990) 1138.

[15] P.S. Hagan, SIAM J. Appl. Math. 42 (1982) 762;
    I. Aranson, L. Kramer and A. Weber, The theory of motion of spiral waves in oscillatory media, in: Spatiotemporal Patterns in Nonequilibrium Systems, P.E. Cladis and P. Palffy-Muhoray, eds. (Addison-Wesley, Reading, MA, 1994); Phys. Rev. E 47 (1993) 3231.

[16] I. Aranson, L. Aranson and L. Kramer, Phys. Rev. A 46 (1992) R2992.

[17] I. Aranson, L. Kramer and A. Weber, Phys. Rev. Lett. 72 (1994) 2316.

[18] H. Chaté and P. Manneville, Defect turbulence and frozen states in the two-dimensional complex Ginzburg–Landau equation; and: Phase turbulence in the complex Ginzburg–Landau equation, to be published.

[19] B. Levitan and E. Domany, Topological model of soap froth evolution with deterministic T2-processes (1995) preprint.

[20] C.C. Chow and T. Hwa, Physica D 84 (1995) 494.

[21] G. Huber, P. Alstrøm and T. Bohr, Phys. Rev. Lett. 69 (1992) 2380;
    G. Huber, Vortex solids and vortex liquids in a complex Ginzburg–Landau equation, in: Spatiotemporal Patterns in Nonequilibrium Systems, P.E. Cladis and P. Palffy-Muhoray, eds. (Addison-Wesley, Reading, MA, 1994).

[22] H. Chaté and L-H. Tang, unpublished.

[23] M. Rost and J. Krug, Physica D 88 (1995) 1.

[24] C.S. Bretherton and E.A. Spiegel, Phys. Lett. A 96 (1983) 152.

[25] See [28] and the discussions in: M.S. Bourzutschky and M.C. Cross, Chaos 2 (1992) 173;
    J. Miller and D.A. Huse, Phys. Rev. E 48 (1993) 2528.

[26] G. Grinstein, C. Jayaprakash and R. Pandit, Physica D 90 (1996) 96.

[27] M. Kardar, G. Parisi and Y.-C. Zhang, Phys. Rev. Lett. 56 (1986) 889;
    see also the reviews: J. Krug and H. Spohn, Kinetic roughening of growing surfaces, in: Solids Far From Equilibrium, C. Godrèche, ed. (Cambridge Univ. Press, Cambridge, 1991);
    T. Halpin-Healy and Y.C. Zhang, Phys. Rep., to appear.

[28] V. Yakhot, Phys. Rev. A 24 (1981) 642;
    S. Zaleski, Physica D 34 (1989) 427;
    K. Sneppen, J. Krug, M.H. Jensen, C. Jayaprakash and T. Bohr, Phys. Rev. A 46 (1992) 7351;
    I. Procaccia, M.H. Jensen, V.S. L'vov, K. Sneppen and R. Zeitak, Phys. Rev. A 46 (1992) 3220;
    V.S. L'vov and I. Procaccia, Phys. Rev. Lett. 69 (1992) 3543;
    C. Jayaprakash, F. Hayot and R. Pandit, Phys. Rev. Lett. 71 (1993) 12.